

**Interface Shapes in Microfluidic Porous Media
Conditions Allowing Steady, Simultaneous Two-Phase Flow**

Cox, S. J.; Davarpanah, A.; Rossen, W. R.

DOI

[10.1007/s11242-023-01905-9](https://doi.org/10.1007/s11242-023-01905-9)

Publication date

2023

Document Version

Final published version

Published in

Transport in Porous Media

Citation (APA)

Cox, S. J., Davarpanah, A., & Rossen, W. R. (2023). Interface Shapes in Microfluidic Porous Media: Conditions Allowing Steady, Simultaneous Two-Phase Flow. *Transport in Porous Media*, 147(1), 197-216. <https://doi.org/10.1007/s11242-023-01905-9>

Important note

To cite this publication, please use the final published version (if applicable).
Please check the document version above.

Copyright

Other than for strictly personal use, it is not permitted to download, forward or distribute the text or part of it, without the consent of the author(s) and/or copyright holder(s), unless the work is under an open content license such as Creative Commons.

Takedown policy

Please contact us and provide details if you believe this document breaches copyrights.
We will remove access to the work immediately and investigate your claim.



Interface Shapes in Microfluidic Porous Media: Conditions Allowing Steady, Simultaneous Two-Phase Flow

S. J. Cox¹ · A. Davarpanah¹ · W. R. Rossen²

Received: 10 August 2022 / Accepted: 17 January 2023 / Published online: 4 February 2023
© The Author(s) 2023

Abstract

Microfluidic devices offer unique opportunities to directly observe multiphase flow in porous media. However, as a representation of flow in geological pore networks, conventional microfluidics face several challenges. One is whether steady simultaneous two-phase flow through a two-dimensional network is possible without fluctuating occupancy of the pore constrictions. Flow without fluctuations can occur only if the flow paths of the two phases can cross on the 2D network; this requires that wetting phase can form a bridge across the gap between grains at a pore constriction while non-wetting phase flows through the constriction. We consider the conditions under which this is possible as a function of the local capillary pressure and the geometry of the constriction. Using the Surface Evolver software, we determine conditions for stable interfaces in constricted geometries, the range of capillary pressures at which bridging can occur, and those where the wetting phase would re-invade the constriction to block the flow of the non-wetting phase (“snap-off”). If a constriction is long and either straight or uniformly curved, snap-off occurs at the same capillary pressure as bridging. For constrictions of concave shape, which we represent as constrictions between cylindrical grains, however, we find a range of capillary pressures at which bridging is stable; the range is greater the narrower the diameter of the cylinders (i.e. the more strongly concave the throat) relative to the width of the constriction. For smaller-diameter pillars, the phenomenon of “Roof” snap-off as non-wetting phase invades a downstream pore body, is predicted not to occur.

Keywords Porous media · Interfaces · Capillary pressure · Snap-off

1 Introduction

Microfluidic devices, or micromodels (Haghighi et al. 1994), are useful for the study of flow in subsurface (geological) porous media (Cha et al. 2020; Chen and Wilkinson 1985; Cui and Babadagli 2017; Gunda et al. 2011; Gutiérrez et al. 2008; Haghighi et al. 1994; Jahanbakhsh et al. 2020; Joekar-Niasar and Hassanizadeh 2012; Karadimitriou

✉ S. J. Cox
sxc@aber.ac.uk

¹ Department of Mathematics, Aberystwyth University, Ceredigion SY23 3BZ, UK

² Delft University of Technology, Delft 2628CD, The Netherlands

et al. 2013; Karadimitriou and Hassanizadeh 2012; Kennedy and Lennox 1997; Kovscek et al. 2007; Marchand et al. 2017; Roman et al. 2016; Tang et al. 2019; Zhao et al. 2016). They have the distinct advantage that one can see the flow dynamics directly, allowing observation of interfacial interactions, mass-transfer processes, phase behaviour, and wetting transitions, for example. Such insights are likely to be of use in understanding the dynamics of fluids in a range of subsurface applications such as oil recovery (Chen and Wilkinson 1985; Cui and Babadagli 2017; Haghighi et al. 1994; Marchand et al. 2017), aquifer remediation (Joekar-Niasar and Hassanizadeh 2012; Karadimitriou and Hassanizadeh 2012; Kennedy and Lennox 1997), and carbon capture and storage (Kazemifar et al. 2016; Morais et al. 2020).

A microfluidic porous medium typically has a geometry consisting of channels of uniform depth bounded by vertical walls. Viewed from above, as in the examples in Fig. 1, the network can have nearly any (2D) shape desired. We call solid barriers to flow (defined by vertical walls) “grains”, and consider two-phase flow consisting of a non-wetting phase (NWP) and a wetting phase (WP). Wetting phase occupies some pores and non-wetting phase others. In those pores that it occupies, NWP occupies the interior of the channels, while WP occupies the corners where grains meet near the top and bottom surfaces (Fig. 2a). WP also coats the solid walls with a film of molecular dimensions (Ransohoff and Radke 1989b). In a complex network of channels, there will be narrower and wider regions: we call the narrow regions “pore throats” and the wider regions “pore bodies”. Multiple pore throats may connect to one pore body in a network. For simplicity, we assume here nearly perfect wetting of the solid by WP.

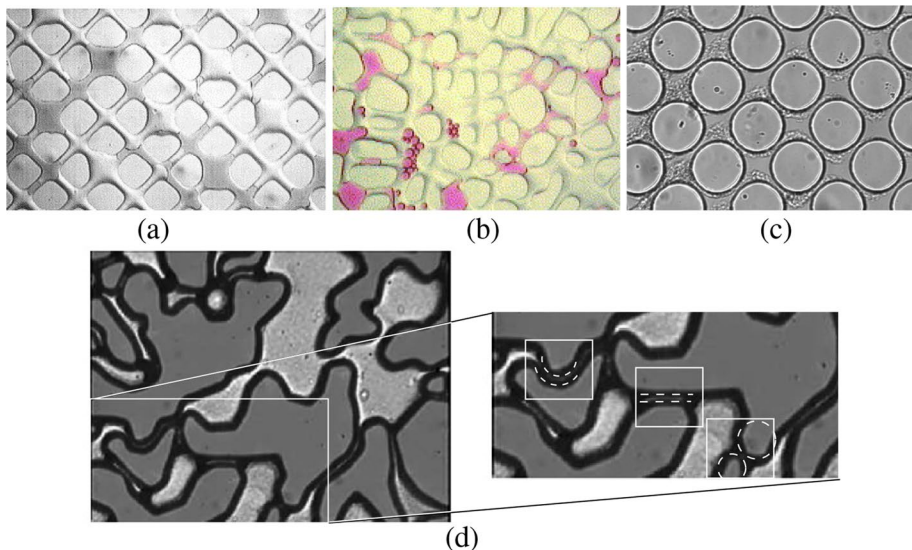


Fig. 1 Examples of microfluidic networks representing an idealized porous medium. **a** Highly ordered (reprinted from Jeong and Corapcioglu (2003), with permission from Elsevier). **b** Disordered artificial network [reprinted from Jeong and Corapcioglu (2003), with permission from Elsevier]. **c** Example of network with concave pore throats between cylindrical grains [reprinted from Perez et al. (2022), with permission from Elsevier]. **d** Network based on a cross section of rock [reprinted from Kovscek et al. (2007), with permission from Elsevier], with one region magnified to illustrate three different channel shapes: straight channel (centre), curved channel (left) and a throat between approximately cylindrical grains (right)

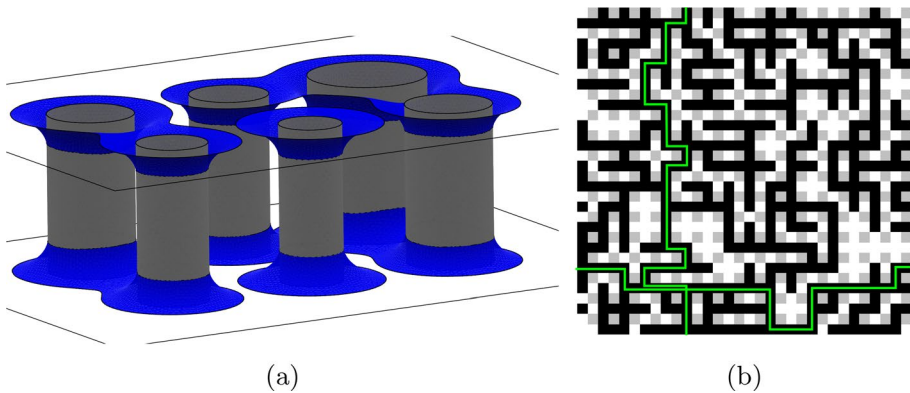


Fig. 2 Phase distributions in a microfluidic network. **a** An example of part of a network in which WP (blue) surrounds the bases and tops of cylindrical grains between parallel plates, while non-wetting phase can flow throughout the interior. WP has bridged the gap between some of the grains, but there is no path for WP to flow from left to right. The film of WP coating the plates and the cylinder walls is not shown, for clarity. **b** Example of invasion percolation on a network of coordination number four, after Holstvoogd (2020). Black is NWP, grey squares represent grains (which could have any shape), white is WP. Periodic boundary conditions apply to top and bottom, and left and right edges. Capillary pressure is sufficient for NWP to enter roughly 50% of pore throats. This is just past the point where NWP can flow from both top to bottom and left to right (possible flow paths are marked with thin green lines). Note there is no path for WP flow from either top to bottom or left to right without crossing the NWP path (i.e. bridging)

Despite the relative simplicity of a 2D microfluidic network, there are many similarities to 3D pore networks in geological formations. These include non-uniform channels/pores, and in particular the presence of pore throats, where capillary forces are significant. Moreover, it is possible to control and adjust the wettability, e.g. by treating surfaces/coating walls with specific minerals (Jahanbakhsh et al. 2020), and to capture a wide range of possible pore geometries. It is also possible to get multiple 3D layers of pores using 3D printing; we do not discuss such networks further here.

Nonetheless, care is needed in extrapolating directly from flow in microfluidics to flow in other porous media. In particular, although the network itself is two-dimensional (2D), the channels are of course 3D.

Percolation theory states that in a truly 2D network, simultaneous, steady two-phase flow is not possible: if flow is to occur then each phase must take turns occupying pore bodies and/or throats (Fisher 1961; see also Sahimi 1994). An example is shown in Fig. 2b: the non-wetting phase (NWP, black) has a path across the network, but not the wetting phase (WP, shown in white). For WP to flow across a 2D network, it must displace NWP from at least one location to make its own path. This then prevents the flow of NWP; for it to flow, it must re-take that location.

Simultaneous quasi-static two-phase flow is possible in 3D geological networks, without fluctuating occupancy of the pore throats; this is an essential aspect of flow in those networks (King and Masihi 2019; Roman et al. 2016; Sahimi 1994; Heiba et al. 1992; Selyakov and Kadet 1996). This reflects the interconnected, interpenetrating flow networks of wetting and non-wetting phases (Valvatne and Blunt 2004). Recent research using micro-CT imaging shows fluctuating pore occupancy at moderate capillary number, but not at low capillary number (Gao et al. 2020; Zhang et al. 2021).

In a microfluidic network, however, it is possible for the wetting phase to cross a throat at top and bottom and connect wetting phase residing in corners around two grains. We call

this a “bridge” (illustrated below): it means that the flow paths of WP and NWP can cross in a microfluidic device.

Our focus here is on the possibility of quasi-static two-phase flow. Two-phase flow is established by injecting both WP and NWP at a fixed ratio into a network occupied by one phase. Reaching the phase distribution for steady two-phase flow involves drainage and imbibition processes, as follows. If a 3D geological pore network is initially fully saturated with WP, quasi-static two-phase flow is established upon sufficient drainage by NWP. Nonzero relative permeability applies to both phases after this drainage process (Blunt 2017; Lake et al. 2014; Øren et al. 1998; Peters 2012; Sahimi 1994; Shikhov and Arns 2015; Valvatne and Blunt 2004; Wu et al. 2017; Zhang et al. 2021). If a microfluidic network is initially full of WP then initially NWP cannot flow across the network; its saturation (the volume fraction in the pore space) and capillary pressure p_c therefore rise until NWP can form a continuous path through the network, as illustrated in Fig. 2b. During drainage of wide pore bodies through narrow pore throats, WP may re-invade and block the throat: this is “Roof snap-off” (Cha et al. 2020; Ransohoff et al. 1987; Ransohoff and Radke 1989b; Roman et al. 2017; Roof 1970; Mohanty et al. 1987). As drainage continues, in the absence of surfactant to stabilize WP films (Joekar-Niasar and Hassanizadeh 2012; Roof 1970), NWP would then re-invade the throat and re-establish connection with NWP in the downstream pore body.

At the point where NWP has established a flow path across the network, the local capillary pressure is too high for bridging, and the WP has no path for flow through the network. WP therefore accumulates, and the average capillary pressure falls, until either bridging occurs at enough throats that WP can flow at the injected fractional flow, or WP fully occupies pore throats, blocking them to the flow of NWP. If this occurs, there is fluctuating occupancy of pore throats, as WP and NWP, each in turn, establishes its path across the network. In this article, we determine the conditions under which bridging of the wetting phase is possible.

The imposition of simultaneous two-phase flow in a 2D network initially saturated by one phase is discussed by Hashemi et al. (1998, 1999a, 1999b). In a 2D network, it results in fluctuating pore occupancy; here we investigate whether the formation of bridges in a microfluidic network might avoid this result. The process of drainage followed by imbibition is not needed to establish simultaneous two-phase flow in 3D pore networks (King and Masihi 2019; Sahimi 1994; Heiba et al. 1992; Selyakov and Kadet 1996). Rather, in quasi-static drainage NWP can establish a flow path without completely blocking the flow of WP. A pressure gradient is of course necessary to drive flow in each phase; in the quasi-static limit, this pressure gradient can be arbitrarily small. In the tortuous paths of each phase through the network (Fig. 2b), the pressure gradient for each phase is not uniform along the network, nor is it necessarily the same in each phase at each location. This implies that capillary pressure is not uniform in the network. In our analysis below, we do not assume uniform capillary pressure in the network, but ask whether any local capillary pressure can stabilize a bridge across a pore throat of given geometry.

Most studies of two-phase flow in microfluidic devices involve injection of one phase to achieve residual saturation of the other phase (Kazemifar et al. 2016; Roman et al. 2016; Jahanbakhsh et al. 2020; Morais et al. 2020). Roman et al. (2016) report that “flow is highly oscillatory” in their experiments and that “the dynamics are accompanied by abrupt changes of velocity magnitude and flow direction”. Marafini et al. (2020) report differences between single-phase flow in microfluidics and 3D pore networks based on numerical studies. Gutiérrez et al. (2008) conducted experiments with simultaneous injection of two phases, and observed flow of discontinuous non-wetting

phase at all flow rates, and relative permeability curves that depend on capillary number. Kovscek et al. (2007) co-injected gas and surfactant solution and observed continuously fluctuating pore-throat occupancy and ascribed it to Roof snap-off. Our goal is to determine whether quasi-static two-phase flow without such fluctuations is possible in common microfluidic networks, as it is in 3D pore networks.

Consider a long, straight pore throat with a uniform rectangular cross section, in which WP lines the corners of the throat (as in Fig. 3b). (By “long” we mean that the interface shape in the middle of the channel depends only on the channel cross section, unaffected by the shape of the pore bodies on either side.) The interfaces between the phases are cylindrical and make contact when (in the case of perfect wetting) their diameter is equal to the width of the channel. That is, bridging across the throat can occur if the throat is at least as tall as it is wide. As the two interfaces then approach each other in the centre of the throat, there is no change in interface curvature (see Sect. 3.1). The value of the capillary pressure p_c at which bridging occurs is, therefore, the same as that for WP to swell and block the whole throat (Rossen 2008). This is what we call “snap-off”, as illustrated in Fig. 4. Snap-off has been studied extensively in various geometries, especially in the context of foam generation (Cha et al. 2020; Kovscek et al. 2007; Ransohoff et al. 1987; Ransohoff and Radke 1989a, b; Roof 1970; Rossen 2008; Wu et al. 2017). In other words, once bridging occurs in a long straight rectangular pore throat, any slight reduction in the capillary pressure in the surrounding medium would cause snap-off in the throat; any slight increase in capillary pressure would cause the bridge to disconnect.

If, instead, the pore throat is not straight, but passes between curved walls (either with the same or opposite curvature) then the curvature of the grain walls affects the conditions for both bridging and snap-off. In this study, we examine conditions (specifically, the range in capillary pressure) for which bridging is possible without snap-off, as a function of throat geometry. We then discuss the implications for the feasibility of two-phase flow without fluctuating pore occupancy in microfluidic devices: that is, the extent to which microfluidic devices are able to represent this aspect of multiphase flow in geological porous formations under capillary-dominated conditions.

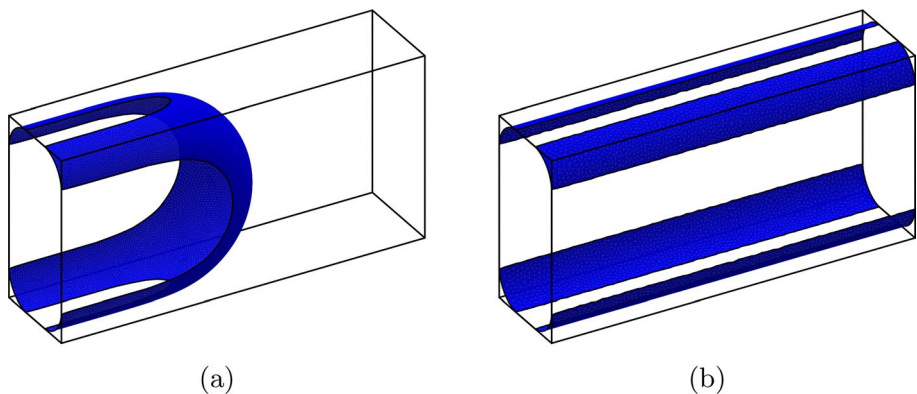
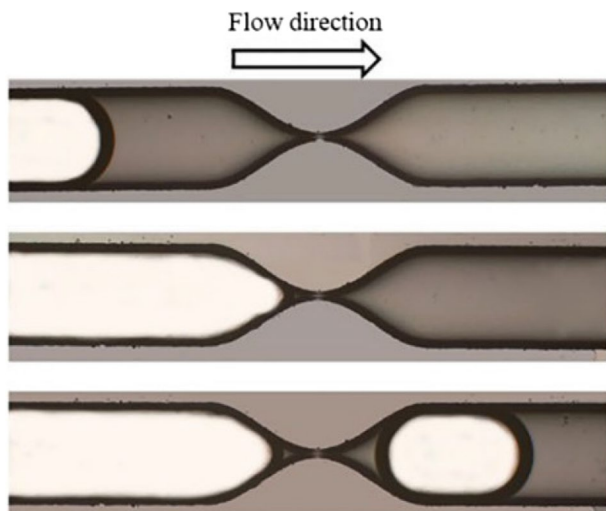


Fig. 3 **a** The interface separating NWP from WP moves from left to right along a straight rectangular channel after overcoming the capillary entry pressure. **b** After the front has left the channel, it leaves behind four narrow regions of WP. The wetting films on the walls are not shown. The channel is twice as high as it is wide and the contact angle is 2°

Fig. 4 Roof snap-off in a constricted rectangular channel, reprinted from Cha et al. (2020) with permission



Before it can penetrate a pore throat, NWP must first overcome the capillary entry pressure p_c^e . Lenormand et al. (1983) predict (in the case of perfect wetting) that the capillary entry pressure in a rectangular channel of cross-sectional width W and height H is

$$p_c^e = \gamma \left(\frac{2}{W} + \frac{2}{H} \right), \quad (1)$$

where γ is the interfacial tension. Including the dependence of capillary entry pressure on contact angle θ (Lago and Araujo 2001) gives, in our notation, the exact result

$$p_c^e = \gamma \left(\frac{1}{W} + \frac{1}{H} \right) \cos \theta \left(1 + \sqrt{1 - \frac{WH}{(W+H)^2} \left[4 \cos \theta (\cos \theta - \sin \theta) - \pi \left(1 - \frac{\theta}{45^\circ} \right) \right]} \right). \quad (2)$$

NWP then moves downstream, displacing WP (the process of drainage; Chen and Wilkinson 1985; Paterson 1984), with the interface at the leading edge advancing steadily along the channel; see Fig. 3a. In the corners behind this moving front, regions of WP remain. The volume of these regions is determined by the curvature of the interface, which itself depends on the aspect ratio of the channel, as well as the contact angle.

Once the front has fully penetrated the channel, just the thin regions of WP in the corners remain; see Fig. 3b. Subsequent drainage or imbibition then causes these regions to shrink or enlarge, respectively. In a long straight channel, all four WP regions in the corners have identical cross section and are uniform along the channel. Ma et al. (1996) relate the capillary pressure of these regions to the shape of the channel and the contact angle θ :

$$p_c = \frac{2\gamma}{\sqrt{A_s}} \sqrt{\sqrt{2} \cos \theta \cos (\theta + 45^\circ) - \frac{\pi}{2} \left(1 - \frac{45^\circ + \theta}{90^\circ} \right)}, \quad (3)$$

where A_s is the cross-sectional area of each region.

If imbibition occurs after the front has left the network, the corner channels swell, and if they become large enough they touch: if this occurs at the bottom or top of the channel, we refer to it as horizontal bridging. If it occurs on the sides of the channel we refer to it as

vertical merging. Vertical merging does not enable WP flow across the throat, since it only connects WP attached to the same grain.

We use the Surface Evolver software (Brakke 1992) (see Sect. 2) to predict the shape of the interfaces in various geometries by minimizing the surface energy of the interface between the two fluids to give an accurate determination of the capillary pressure p_c (the pressure difference across the interface, calculated by the program). By making small changes in the NWP volume and repeating the minimization, we predict the quasi-static variation of capillary pressure during imbibition or drainage. As well as neglecting viscous losses, we assume that the effects of gravity are negligible on the scale of the channels.

We establish a benchmark for our simulations in a straight rectangular channel, determining the effect of the choice of channel aspect ratio and the contact angle at which the interfaces meet the walls of the channel (Sect. 3.1). We then modify this channel to allow both side walls of the grains to have curvature: either in the same direction, giving a curved rectangular “duct” (Sect. 3.2), or in opposite directions, giving a flow between cylindrical grains (Sect. 3.3) into a large pore body downstream. We use this geometry to also represent the larger class of throats of concave shape, as viewed from above.

The channel height H is uniform in most microfluidic devices. We normalize lengths by $H/2$ and normalize capillary pressures by the capillary entry pressure of a Hele-Shaw cell, i.e. a gap between two smooth, parallel plates: $p_{\text{cd}} = p_c/(2\gamma/H)$. In the following, we mostly consider the case $W = H/2$, for which Eq. (1) predicts $p_{\text{cd}}^e = 3$. For a surface tension of $\gamma = 3 \times 10^{-2} \text{ N/m}$ and a channel height $H = 25 \mu\text{m}$, the corresponding dimensional capillary pressure is $p_c \approx 7200 \text{ Pa}$.

The trends in capillary (entry) pressure with varying H , W and θ for straight ducts are captured well by Eqs. (2) and (3), and so here we concentrate on the variation with changes in wall curvature.

2 Simulation Method

The Surface Evolver program minimizes surface energy by moving the interface between WP and NWP, subject to a fixed solid geometry and fixed phase volumes. In this case, the surface energy is the surface area of the interfaces multiplied by their surface tensions. Each interface is tessellated into many small triangles to allow it to curve; we generally use four levels of refinement (i.e. recursive splitting of one triangle into four smaller triangles) to provide an acceptable level of accuracy without simulations taking more than a few hours to explore all relevant parameter values.

The software explicitly accounts for the surface energies of each phase against solid walls and also against each other; by adjusting the solid/fluid phase surface energies, we can in effect fix the contact angle. The difference in interfacial tension between where NWP and WP touch the solid walls, γ_w , sets the contact angle, $\theta = \cos^{-1}(\gamma_w/\gamma)$. In the absence of gravity, the value of the interfacial tension is not important to interface shape, only the ratio γ/γ_w .

The case of perfect wetting—a contact angle of 0° —is numerically slow to converge, so we mostly employ a small contact angle of a few degrees which ensures that simulations converge quickly and accurately. We show below that the prediction of capillary pressure with a contact angle of 2° is almost indistinguishable from perfect wetting.

At the entrance and exit of the channel, represented as vertical planes, we set the contact angle to 90° . This in effect gives a plane of symmetry to the fluid interface at the entrance

and exit of the channel. This does lead to an unphysical artefact for small NWP volumes at the entrance: NWP forms a hemisphere of small radius until its volume is large enough that it touches the solid walls of the channel. This in turn implies a large capillary pressure before NWP fully penetrates the throat. Therefore, in the results below, we show only calculations after NWP volume is large enough to press against the solid walls at the entrance.

Surface Evolver then allows us to calculate the capillary pressure, the spatial distribution of fluid phases, and the stability of the interfaces. We fix the volumes of WP and NWP and incrementally reduce WP volume to simulate quasi-static penetration of the channel by NWP or increase WP volume to simulate re-imbibition. Symmetry can be used to speed up the calculations: for example, it is only necessary to simulate one quarter of the straight channel, since all four corners are equivalent.

To determine the stability of the interface, we examine the eigenvalues of the Hessian matrix of the energy (Brakke 1996): a change in the sign of the smallest eigenvalue to a negative value signals instability. The software includes tools that allow us to determine the corresponding eigenmode, which indicates the nature of the instability.

In a straight channel with a rectangular cross section (Fig. 3) there are side walls at $x = \pm \frac{1}{2}W$, with the bottom at $z = 0$ and the top at $z = H$, the entrance at $y = 0$ and exit at $y = L$. A channel length of $L = 2H$ is sufficient for a steadily propagating interface to form during drainage. The side walls are replaced by parts of a cylinder of radius $R_{\text{curv}} \pm \frac{1}{2}W$ to generate a curved rectangular duct. Finally, cylindrical grains with radius R are placed at $x = \pm \left(\frac{1}{2}W + R\right)$, $y = 0$ between a flat base to the channel at $z = 0$ and a flat top at $z = H$.

As noted above, establishment of paths for simultaneous, quasi-static two-phase flow in a microfluidic network requires first drainage and then imbibition. We first simulate drainage of the throat, and then imbibition, as follows. Consider for example a meniscus of WP around the bases of two nearby cylindrical grains (see Fig. 2a) with NWP everywhere else in the throat and filling the pore bodies on either side. At first WP occupies only the corners around the grains, but as we increase WP volume these menisci spread outwards and the capillary pressure falls. In Sect. 3.3, we determine the point at which the two WP regions connect, bridging the throat, and record the corresponding capillary pressure p_c^{br} . As its volume is increased further, WP rises up the sides of the grains and the throat is slowly filled with WP from above and below. When WP reaches half-way up the grains, it meets the menisci coming down from above. At this point, there is an instability (negative eigenvalue) associated with an eigenmode indicating contraction of the interface towards the centre of the channel. We identify this as snap-off and this value of the capillary pressure p_c^{sn} as that for snap-off. We can take the Surface Evolver calculations no further beyond this change in the topology of the interfaces.

3 Results

3.1 Straight Channel

Figure 5a shows the capillary entry pressure in a straight rectangular channel with aspect ratio $H = 2W$ as a function of contact angle. As noted above, a contact angle of less than 5° gives a good approximation to the result for perfect wetting. This is just below the prediction of Eq. (1) for the capillary entry pressure.

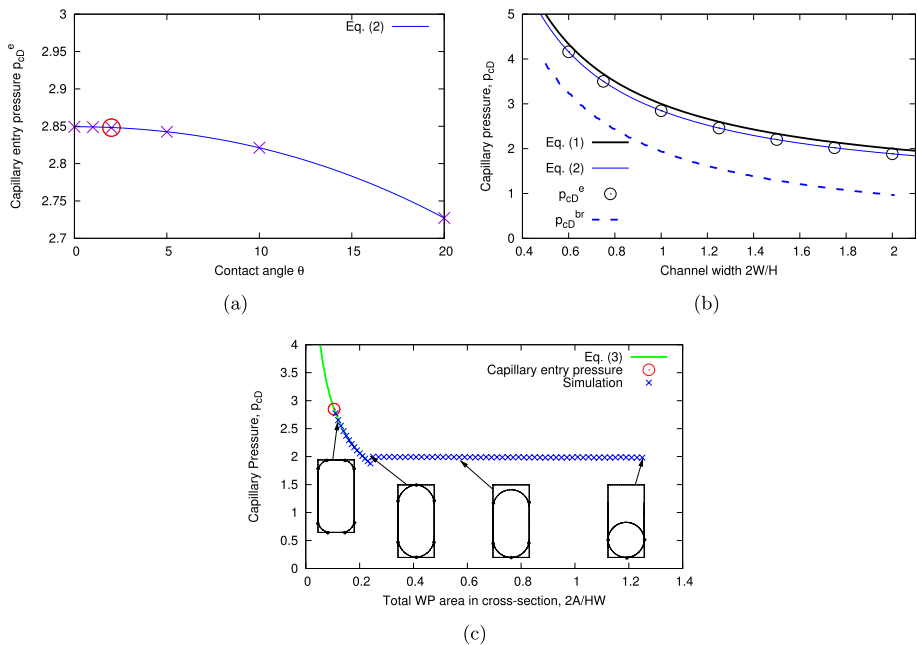


Fig. 5 Capillary pressure in straight rectangular channels. **a** Capillary entry pressure for different contact angles in a channel with $H = 2W$. The value of the capillary entry pressure for different contact angles is almost indistinguishable for θ less than about 5° , justifying our use of a small finite contact angle of 2° (highlighted with a circle) in the following. The steady advance of the interface through the channel occurs with capillary pressure slightly less than the prediction of Eq. (1), $p_{cD}^e = 3$, and our data is in agreement with Eq. (2). **b** Capillary entry pressure as a function of channel width with fixed channel height and contact angle 2° . The capillary entry pressure is slightly over-estimated by Eq. (1), while the capillary pressure at which bridging (and consequent snap-off) occurs is lower than p_{cD}^e . The capillary pressure is greatest for a tall, narrow channel. **c** Capillary pressure as a function of the total area of WP that remains in the cross section of a channel with $H = 2W$ after the interface has fully penetrated the channel. The contact angle of $\theta = 2^\circ$ leads to a slight undershoot in p_{cD} in contrast to the case of perfect wetting. Representative interface shapes are shown in the cross section before, at and after bridging, and at snap-off

Figure 5b shows that increasing the width W of the channel (while keeping its height H fixed) reduces the capillary entry pressure, as predicted by Eq. (1). The deviation in the simulated value of the capillary entry pressure from the prediction of Eq. (1) (Lenormand et al. 1983) increases slightly as the channel gets narrower. Bridging occurs in the straight channel when the pair of upper or lower regions of WP (cf. Fig. 3b) meet in the middle of the channel. At this point, the capillary pressure has fallen from the capillary entry pressure; its value also decreases with an increase in channel width, because the volume of WP required for bridging is greater. Moreover, in a straight channel, the capillary pressure for bridging, p_c^{br} , is equivalent to the value for snap-off, p_c^{sn} , since as soon as NWP no longer touches all four walls of the channel a Rayleigh–Plateau instability occurs and NWP breaks up.

Equation (3) gives the value of p_c for any WP volume in a rectangular channel before bridging (since the aspect ratio is irrelevant before the WP regions meet). Figure 5c confirms that our simulations agree with the prediction of Eq. (3). Further, the area of the WP regions in the corners is entirely determined by the shape of the front separating NWP and WP that moves along the channel at the capillary entry pressure, as illustrated in Fig. 3.

3.2 Curved Rectangular Duct

If the channel is a uniformly curved duct with planar top and bottom, as shown in Fig. 6a and Movie 1 in the Supplementary Material, the capillary pressure of an interface moving along the duct is indistinguishable from its value in a straight channel. That is, the radius of curvature R_{curv} of the centreline of the duct (which must be greater than $W/2$) does not influence p_c , at least for the values of $R_{\text{curv}} > 2W$ considered here.

However, the areas of the triangular regions that remain in the corners of the duct after the interface has passed are different on the inner and outer curved walls; their capillary pressure is the same, but the curvature of the walls forces them to adopt different shapes. Figure 6b shows that the cross-sectional area of these regions can deviate significantly from the straight-channel case (in which the inner and outer WP regions are identical), with a greater deviation on the inner wall. However, they slowly converge towards the same value as the radius of curvature R_{curv} increases.

If, after the interface has passed through, WP re-imbibes into the channel, then two of the four triangular regions may meet. There are two cases to consider. First, if the height H is greater than the width W , as is the case in our “standard” channel here, then bridging first occurs at the top and/or bottom of the duct. However, at the same capillary pressure WP flows in and the interfaces then merge on the outer wall, as shown in Fig. 7. Second, if the width W is at least as great as the height H (a shallow, wide channel), the order in which the transitions occur is reversed: the interfaces first merge on the outer wall, furthest from the centre of curvature, and then bridge across the top and/or bottom of the duct.

Figure 7 appears to show that there is a narrow range of capillary pressure in which a bridge is stable, from $p_{\text{cD}} \approx 1.9$ to 2.0. However, this is an artefact of using a finite contact angle in the calculations, as illustrated schematically in Fig. 7b. If we use a contact angle of 5° instead of 2° , the region extends down to $p_{\text{cD}} \approx 1.83$, but it vanishes in the limit of zero contact angle. More fundamentally, the overshoot in capillary pressure in Fig. 7 indicates instability to snap-off in the throat for nonzero contact angle. If the

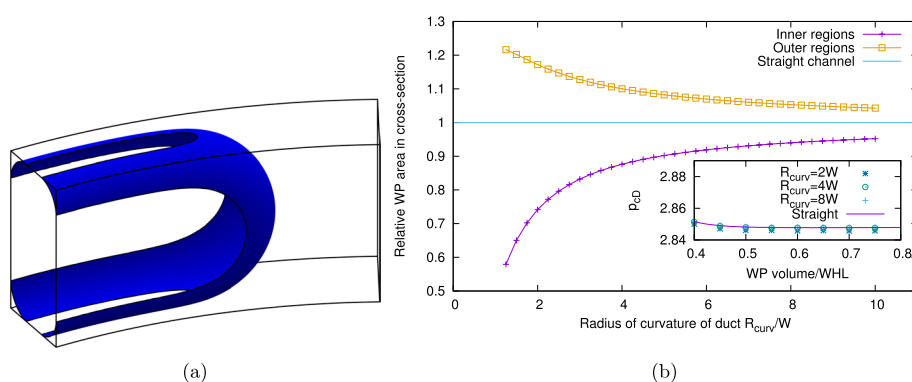


Fig. 6 **a** Penetration of NWP into a curved rectangular duct with $H = 2W$ and $R_{\text{curv}} = 8W$, i.e. with curved walls having radius of curvature $(R_{\text{curv}} \pm \frac{1}{2}W)$. The interface separating the two fluids meets the walls at a contact angle of 2° . **b** Cross-sectional area fractions of the WP regions in the corners of a curved rectangular duct, normalized by the value for a straight channel of the same width and height. The inset shows that the capillary entry pressure is independent of the radius of curvature of the duct, at least for $R_{\text{curv}} \geq 2W$. The contact angle is 2°

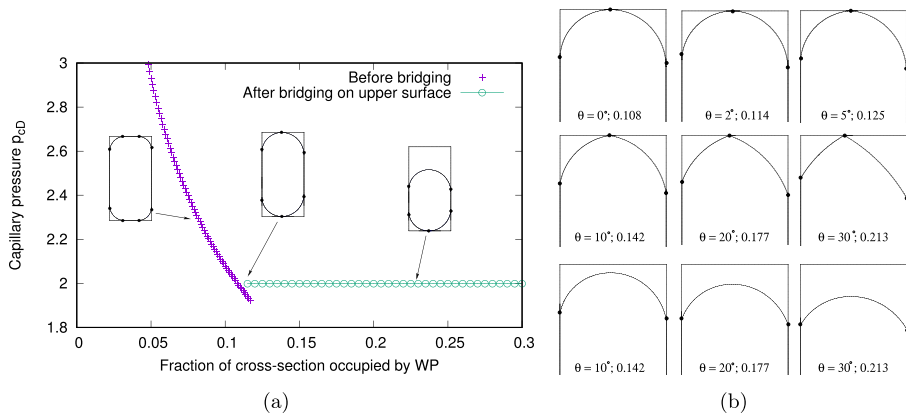


Fig. 7 Imbibition into a curved rectangular duct with $H = 2W$ and radius of curvature $R_{\text{curv}} = 5W$. **a** The capillary pressure decreases until the first bridge is formed: if the channel height is greater than its width this occurs first on the top (as shown) or bottom surfaces. The interface then remains in contact with three walls and the capillary pressure does not change until the merging transition on the outer wall. Also shown is the sequence of interface shapes in a vertical cross section through the duct, with points at which the interface meets the duct surfaces highlighted with dots. The contact angle is 2° , which gives rise to a slight undershoot in p_c in contrast to the case of perfect wetting. **b** Interface shapes in a vertical cross section through the upper half of the duct immediately before and after bridging. Images are labelled with the contact angle θ , measured in degrees, and the fraction of the cross section occupied by WP. The top two rows show the interface immediately before bridging for contact angles up to 30° . The bottom row shows the shape of the (unstable) interface immediately after bridging for contact angles between 10° and 30° . This explains why nonzero contact angles lead to an undershoot in p_c : the radius of curvature at the point where the two WP regions meet is greater just before the two regions bridge than it is after

capillary pressure of the network were low enough for bridging in the given throat, WP would flow into that throat spontaneously from the surrounding network to fill it at the higher capillary pressure.

With $H = 2W$, bridging across the top or bottom of the duct occurs at the same area fraction of WP in the cross section of 0.12, and the same capillary pressure ($p_{cD} \approx 2$) for values of the radius of curvature R_{curv} between $2W$ and $8W$ (data not shown). That is, although the wetting phase is re-distributed between the triangular regions on the outer and inner sides of the duct as its curvature changes, and therefore the position at which they meet is different, the critical total volume of WP and the capillary pressure at which the regions meet does not change.

Following bridging, there is an almost semicircular interface (in cross section) moving vertically within the duct (Fig. 7a). The capillary pressure increases very slightly with increasing volume of WP in this regime. Such a situation is unstable, as in the arguments of Roof (1970) concerning the largest inscribed circle, and WP floods into the duct and blocks the flow of NWP. Thus, the merging transition on the outer wall is never observed without snap-off, and the capillary pressure for snap-off is the same as the capillary pressure for bridging: $p_c^{\text{br}} = p_c^{\text{sn}}$.

In the case of a duct with square cross section ($H = W$), the situation is slightly different. The merging transition on the outer wall occurs at a capillary pressure that depends on the radius of curvature: it occurs at higher capillary pressures, and hence lower volumes of WP, in tightly-curved wide ducts. After merging, the capillary pressure increases slightly, as in Fig. 7a, and so snap-off occurs and WP floods into the duct.

3.3 Throat Between Cylindrical Grains

Thus in both the straight and curved rectangular channels with aspect ratio $H = 2W$, the capillary pressure at which bridging occurs is the same as the capillary pressure for snap-off. We now consider a situation in which the curvature of the side walls has a different sign on each side, and show that in this case there is a range of capillary pressure for which bridging without snap-off is stable.

3.3.1 WP Surrounding the Base of Two Grains

As described above, we gradually increase the volume of WP around and in the throat between two cylinders of radius R situated between parallel horizontal plates; one half (by symmetry) of the geometry is shown in Fig. 8a. We fix the height H and vary the radius R of the grains and the throat width W between them and determine the different capillary pressures for bridging and snap-off.

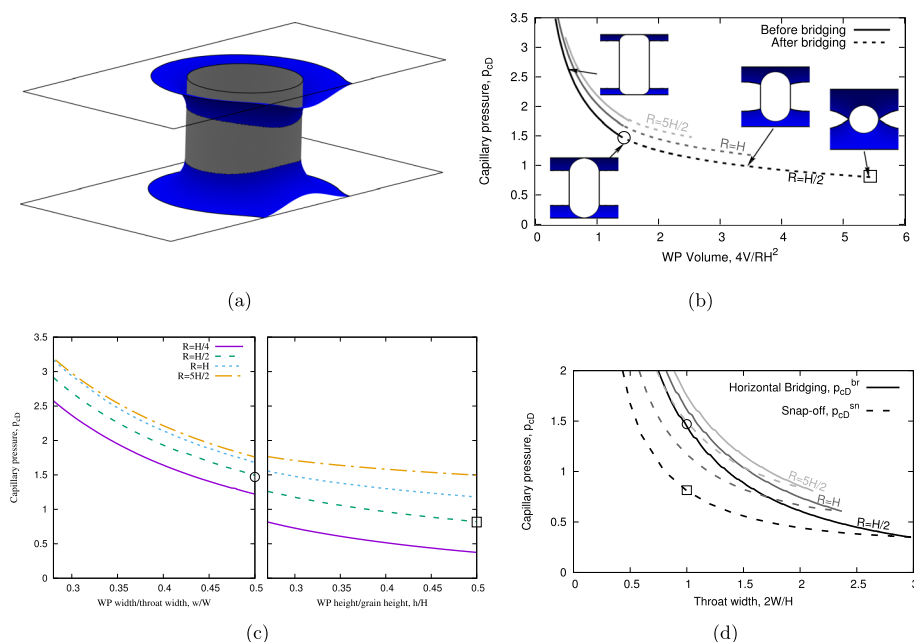


Fig. 8 Bridging and snap-off in a throat between cylindrical grains. **a** Oblique view of WP around one of the two grains, with $R = H/2$, between the formation of the horizontal bridge and snap-off. **b** Capillary pressure as a function of WP volume (normalized by $RH^2/4$), for cylinders of radius $R = H/2, H$ and $5H/2$, with throat width $W = H/2$. The circular symbol indicates bridging and the square symbol indicates snap-off here and in (c) and (d) for the case $R = H/2$. The images are views through the centre of the throat, with w/W reaches 0.5 the WP bridges across the channel. When h/H reaches 0.5 the two regions of WP touching the top and bottom surfaces merge and snap-off occurs. **c** Capillary pressure during imbibition for different grain radii. When w/W reaches 0.5 the WP bridges across the channel. When h/H reaches 0.5 the two regions of WP touching the top and bottom surfaces merge and snap-off occurs. **d** The capillary pressures at which bridging and snap-off occur for various throat widths for grains with radius $R = 1, 2$ or 5 . Vertical merging occurs before bridging for values of throat width greater than the point at which the two curves meet for each value of the grain radius. The contact angle is 2°

It is instructive to first consider the shape of the interface surrounding an isolated pair of cylindrical grains and its capillary pressure. Figure 8 shows images of the interface and the capillary pressure and Movie 2 in the Supplementary Material shows a sequence of interface shapes as WP volume increases.

The regions of WP in the corners at the base and top of each grain extend some distance w across the throat and some height h up the sides of the grains. We use Surface Evolver to calculate the capillary pressure and the values of w and h as the WP volume V varies for different throat widths W , as shown in Fig. 8c, d. The capillary pressure decreases as the WP volume increases and w and h increase. When w reaches $W/2$ the WP bridges the throat; we denote the capillary pressure at which this happens by p_c^{br} . Figure 8b shows that the volume of WP at which bridging occurs increases linearly with grain radius R , but that p_c^{br} increases only slightly with R .

Figure 8c indicates that the capillary pressure decreases further as WP volume increases in the throat. There is a range of p_c for which a bridge is stable without snap-off, corresponding to the difference in capillary pressure between the right-hand edges of the two panels in Fig. 8c for each value of R . The upper and lower WP regions in the throat meet, half-way up the grains, when their height is $h = \frac{1}{2}H$, at which point we denote the critical capillary pressure by p_c^{m} : the right-most values in Fig. 8c. Note that at the point where the bridging between upper and lower WP regions occurs the cross section of the interface appears nearly circular (Fig. 8b, right-most cross section); the gradient of $p_c(V)$ is very shallow here (Fig. 8c, right-hand panel). This indicates that the WP has almost reached the critical point for snap-off, beyond which it floods back into the throat (Ransohoff et al. 1987). Our calculations and assessment of the eigenmodes given by Surface Evolver suggest that this instability occurs immediately as these two regions meet, and that the interface changes topology.

At small throat widths, there is a significant difference between the capillary pressure for bridging and the capillary pressure for snap-off, since bridging can happen at small WP volume but the WP volume must increase significantly before vertical merging occurs. As the throat widens (increasing W , Fig. 8d), more WP must accumulate before bridging occurs. Consequently, the capillary pressure for bridging decreases with increasing throat width.

At large-enough throat widths, above about $W = 3H/2$ in the case $R = H/2$, merging between the top and bottom regions of WP on the grains occurs before horizontal bridging across the throat. This gives rise to a capillary bridge connecting the top and bottom interfaces, but does not permit two-phase flow in the network.

3.3.2 Asymmetric Case

Up until now we have considered a situation in which WP around both grains is at the same capillary pressure. However, when NWP first crosses the pore network, as illustrated in Fig. 2b, the connections between regions of WP are broken. As WP accumulates, the capillary pressure falls, but only in the interconnected network of WP-filled pores connecting back to the point of injection. Therefore, when these critical bridges form, giving a WP connection across the network, one grain is connected to the reservoir of WP at low capillary pressure while the other grain is not. The bridge has to form with WP initially accumulating on one side only.

What happens after the bridge forms? Clearly, the dynamics of bridge formation are complex in the short term, but the final result is that both sides are now at the lower value

of capillary pressure associated with the flowing network of WP. So the question is: what is p_c on the wet grain at the point when the bridge forms? Is it low enough that, once this value of p_c is established on both sides, there would be snap-off?

To investigate this issue, we again use a throat width of $W = H/2$, cylindrical grains of radius $R = H/2$, and assume that the WP meniscus surrounding the dry pillar has capillary pressure close to the capillary entry pressure, $p_{cD} \approx 3$. From the left-hand side of Fig. 8c, we see that WP extends a distance slightly less than $w/W = 0.3$ from the base of the grain in this case. Bridging will therefore occur if the WP around the wet grain extends to a distance of $w/W = 0.7$ from that grain. The capillary pressure around the wet grain at bridging is the value of p_c^{br} for a throat width $W = 1.4H/2$, which Fig. 8d indicates is $p_{cD} \approx 1.0$. This is greater than the capillary pressure for snap-off (Fig. 8b), $p_{cD} \approx 0.8$, and hence bridging will not lead to snap-off in this case.

For snap-off to occur immediately following bridging in this asymmetric case, the extent of the WP meniscus around the dry grain must be smaller than hypothesized, and the WP at higher capillary pressure. The capillary pressure can be greater on the dry grain than the capillary entry pressure for that throat. As NWP invades a pore network filled with WP, as shown in Fig. 2b, capillary pressure rises throughout the network according to the capillary entry pressure of the latest throat to be invaded. As noted above, that process stops when NWP forms a continuous path across the network and WP continuity across the network is broken. Thus, the capillary pressure on the dry grain is at the capillary entry pressure of the last throat to be invaded by NWP, not that of the given throat. Figure 8d indicates that the capillary pressure for snap-off with $W = H/2$ (again with $R = H/2$) is equal to the capillary pressure for bridging at a throat width of $W \approx 1.7H/2$. So only when the WP meniscus around the dry grain extends no more than 15% of the way across the throat, with a capillary pressure of $p_{cD} \approx 5$, far in excess of the capillary entry pressure for that throat, is snap-off without bridging possible.

For larger grain radii, the curves of capillary pressure against throat width are less steep (Fig. 8d), the difference between p_c^{br} and p_c^{sn} smaller (Fig. 8c), and so this transition to snap-off in the asymmetric case becomes more likely and flow without fluctuating pore occupancy less likely. For example, with $R = H$ the value of p_c^{br} drops from its value for bridging at $W = H/2$ ($p_{cD}^{br} \approx 1.7$) to below the value for snap-off at $W = H/2$ ($p_{cD}^{sn} \approx 1.2$) when $W \approx 1.4H/2$, suggesting that snap-off would immediately follow bridging driven from one side.

For larger throat widths, it is more likely that vertical merging would occur before bridging between the grains, something which our calculations do not currently resolve.

3.3.3 Roof Snap-Off: Penetration of NWP Into a WP-Filled Pore Body

Snap-off triggered by NWP invasion of the downstream pore body is called “Roof” snap-off (Ransohoff et al. 1987; Roof 1970; Rossen 2003). We turn now to the invasion of NWP into a WP-filled pore body downstream of the throat, i.e. during initial drainage of the pore network. We fix the throat width to be $W = H/2$. NWP penetrates the pore body with a roughly hemispherical front (Fig. 9a and Movie 3 in the Supplementary Material) and leaves behind narrow regions of WP in the corners of the channel where the grains meet the upper and lower surfaces.

Figure 9b shows the capillary pressure across the interface as it moves through the throat for four different values of the grain radius R (at fixed W). The maximum

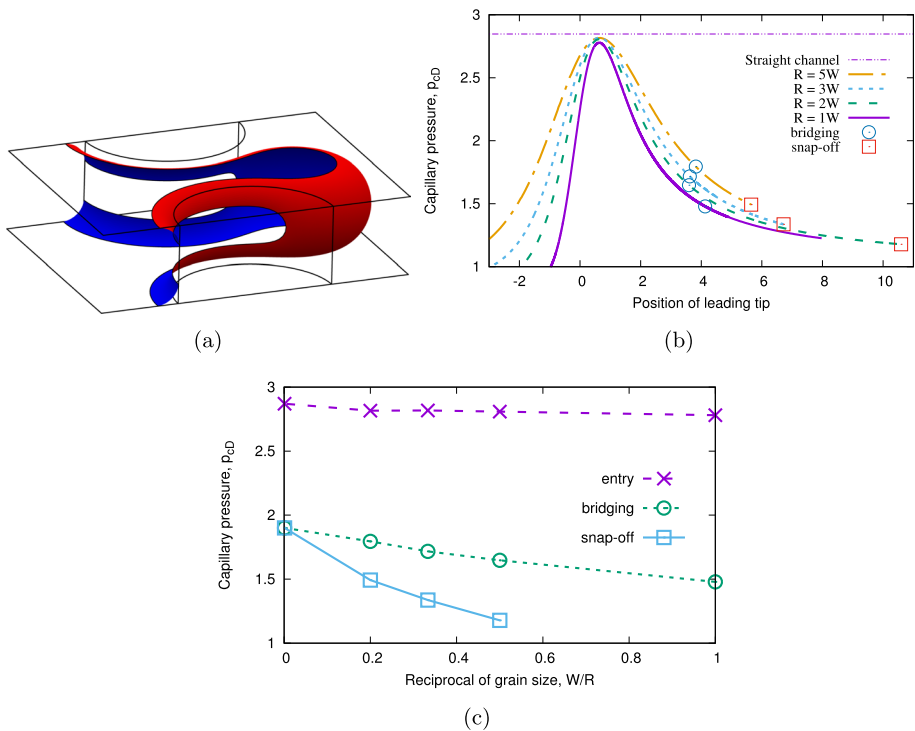


Fig. 9 NWP penetration of the pore throat between grains into a downstream pore body. **a** The interface moves from left to right through the gap between two cylindrical grains, leaving WP around the base and top of each grain. Grain radius is $R = H/2$ in this case. **b** Capillary pressure as a function of the position of the tip of the WP interface, defined relative to the centre of the throat. The maximum capillary pressure occurs just after the leading tip of the interface has passed the centre of the throat. It increases slightly with an increase in radius of the grains. Also shown is the predicted capillary pressure in a straight channel, slightly below the prediction of $p_{cD}^e = 3$ from Eq. (1). We do not find snap-off in the case $R = W$, as discussed in the text. **c** A summary of the different critical capillary pressures, plotted as a function of the inverse of the grain size so that the values for the straight channel are shown on the left. Throat width is $W = H/2$ and the contact angle is 2°

capillary pressure p_c^e is greatest for the widest grains and, for sufficiently large R , p_c^e approaches the value for a straight channel. This maximum occurs just after the front (measured as the leading position on the interface along the axis through the throat) has passed between the grains. Thus, the curvature of the grains affects the curvature of the interface and the value of p_c^e .

After the front has passed through the throat between the grains, the capillary pressure decreases as the NWP spreads out into the pore space beyond. The narrow regions of WP in the corners of the channel shrink and swell as the capillary pressure increases and then decreases as the interface invades the pore throat and then the downstream pore body (see Movie 3 in the Supplementary Material).

We can estimate the horizontal extent of the interface downstream, beyond the grains, as follows. Far downstream of the grains the interface has a nearly semicircular vertical cross section, spanning the gap between the flat upper and lower surfaces (see Fig. 9a). If we also

approximate its horizontal cross section as a circle of diameter D , then the capillary pressure here is $p_{cD} = \left(1 + \frac{H}{D}\right)$, similar to Eq. (1).

The interface must have the same capillary pressure everywhere, so we compare this expression for the capillary pressure to the critical value p_c^{sn} for snap-off in the throat when $h = H/2$. We extrapolate the data shown in Fig. 8c for $p_c^{sn}(h = \frac{1}{2}H)$ to more values of R and then estimate the minimum pore body diameter at which Roof snap-off can occur in the pore throat:

$$D = 2/(p_c^{sn}/\gamma - 2/H). \quad (4)$$

This is shown in Fig. 10a, where it is compared with results for the width of the interface from simulations, such as the one shown in Fig. 9a, that have been allowed to run until the capillary pressure decreases to p_c^{sn} and WP fills the throat: i.e. Roof snap-off.

For gently constricted pores with circular cross section along the flow axis, the criterion for Roof snap-off is that the diameter of the pore body be at least twice the diameter of the throat (Ransohoff et al. 1987). In this case, with $W = H/2$, that suggests $D = H$. In microfluidic devices of uniform depth, pore bodies must be wider than this to trigger Roof snap-off. Strongly convex throats, reflected here in small R , stabilize bridging against snap-off during subsequent imbibition, but may not allow Roof snap-off during initial drainage of the network. The value of D that we predict here is close to the simulated values shown by the black squares in Fig. 10a; it is a small multiple of the throat width for grains with large radius, but rises rapidly for smaller grains, and diverges somewhere between $R = H/2$ and $R = H$. We see that $D \rightarrow \infty$ for $p_c^{sn} \rightarrow 1$, which Fig. 8d indicates is indeed the case for R/H between 0.5 and 1. In all cases, it is much larger than the criterion for pore bodies and throats of circular cross section.

Hence for sufficiently tightly-curved grains (highly convex pore throats), Roof snap-off does not occur during NWP invasion of the pore throat for any size pore body downstream, no matter how wide (viewed from above). The minimum possible grain radius R_{\min} for which Roof snap-off is possible also depends on the throat width. By calculating the cylinder radius at which, for a given throat width W , the capillary pressure for snap-off is equal to $2\gamma/H$, we can determine $R_{\min}(W)$, as shown in Fig. 10b. If the throat is narrow, then Roof snap-off can occur in a sufficiently wide pore body; the minimum grain radius that

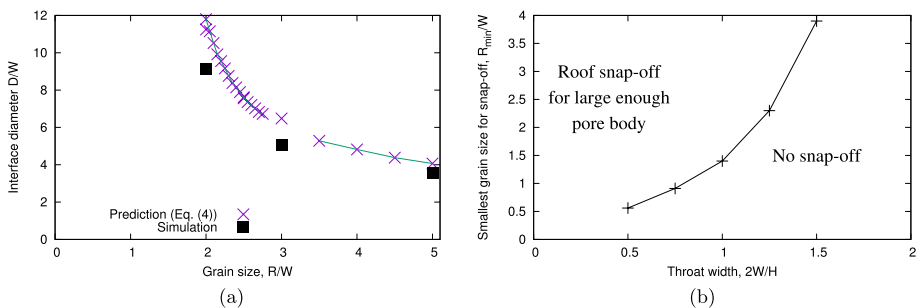


Fig. 10 Implications for Roof snap-off. **a** The diameter of the interface that is created in the pore body downstream when snap-off occurs in the throat: comparison of Eq. (4), using capillary pressure values from Fig. 8, with direct simulation, as in Fig. 9a. throat width is $W = H/2$. **b** The minimum grain radius for Roof snap-off in a throat of given width. Roof snap-off does not occur in the region below the curve because the capillary pressure for snap-off, even for an infinitely wide pore body, is below $2\gamma/H$

can support snap-off increases rapidly as a function of throat width. Cha et al. (2020) present a similar analysis and results for one throat geometry, in terms of a minimum depth of the throat rather than maximum pore body diameter.

4 Conclusions: Implications for Two-Phase Flow in Microfluidics

Our findings can be summarized as follows. Bridging is not possible without snap-off in relatively long straight or curved ducts. Of the examples shown in Fig. 1, (a) features constrictions between pore bodies that are straight, rectangular ducts. Some throats in (b) are nearly straight, while others approximate grains of very large radius. Those in (d) include curved rectangular ducts, straight channels, and some tightly concave throats. Based on these geometries, we conclude that it is unlikely that two-phase flow is possible in the networks shown in Fig. 1, or similar networks, without fluctuating occupancy of locations in the pore space. Gutiérrez et al. (2008) report displacement of ganglia at all flow rates when steady two-phase injection is imposed in their microfluidic apparatus.

In three-dimensional geological pore networks, quasi-static two-phase flow without fluctuating pore occupancy can occur at arbitrarily small pressure gradients (King and Masihi 2019; Sahimi 1994). At higher pressure gradients, quantified through the dimensionless capillary number, flow with fluctuating pore occupancies and displacement of trapped, isolated NWP is possible (Blunt 2017; Lake et al. 2014; Tang et al. 2019). The flow regime above this transition in capillary number differs significantly from that below it (Lake et al., 2014). This suggests that imposing two-phase flow in most current microfluidic devices must necessarily drive the flow into the high-capillary-number regime, with relative permeabilities that depend on capillary number (Gutiérrez et al. 2008; Karadimitriou and Hassanizadeh 2012).

Bridging and steady two-phase flow are possible in networks featuring concave pore throats, represented here by throats between cylindrical grains of narrow radius. In that geometry, as shown in Fig. 8, there is a range of capillary pressure at which bridging is stable without snap-off. For very tightly concave throats, however, Roof snap-off may not be possible, no matter how wide the downstream pore body (Fig. 10). In all cases, the width of a pore body in comparison with the width of a throat, as viewed from above, that would give Roof snap-off is much greater than that for pores and throats of circular cross section (Roof 1970). This suggests that studies of Roof snap-off in microfluidic networks are problematic as a model for 3D pore networks (Kovscek et al. 2007; Rossen 2008).

As illustrated in Fig. 2b, under conditions where both phases might flow, the flow path for each phase is extremely inefficient. That suggests that the relative permeability of each phase (King and Masihi 2019; Lake et al. 2014; Sahimi 1994) is very low. One implication is that even in conditions where steady two-phase flow is possible, the pressure gradient required to sustain the imposed flow rate could push the capillary number above the point where pore occupancy fluctuates. It also could lead to situations where local pressure differences across individual pore throats of one phase blocking the other could be large. This is the subject of ongoing research that will be reported separately.

Supplementary Information The online version contains supplementary material available at <https://doi.org/10.1007/s11242-023-01905-9>.

Acknowledgements We thank K. Brakke for the development and maintenance of the Surface Evolver, and E. Obbens and J. Holstvoogd for their help with creating and analysing 2D networks such as the one shown in Fig. 2b.

Funding This work was supported by an AberDOC PhD scholarship from Aberystwyth University.

Open Access This article is licensed under a Creative Commons Attribution 4.0 International License, which permits use, sharing, adaptation, distribution and reproduction in any medium or format, as long as you give appropriate credit to the original author(s) and the source, provide a link to the Creative Commons licence, and indicate if changes were made. The images or other third party material in this article are included in the article's Creative Commons licence, unless indicated otherwise in a credit line to the material. If material is not included in the article's Creative Commons licence and your intended use is not permitted by statutory regulation or exceeds the permitted use, you will need to obtain permission directly from the copyright holder. To view a copy of this licence, visit <http://creativecommons.org/licenses/by/4.0/>.

References

- Blunt, M.: *Multiphase Flow in Porous Media: A Pore-Scale Perspective*. Press, Cambridge, UK, Cambridge (2017)
- Brakke, K.: The surface evolver. *Exp. Math.* **1**, 141–165 (1992)
- Brakke, K.: The surface evolver and the stability of liquid surfaces. *Philos. Trans. R. Soc. A* **354**, 2143–2157 (1996)
- Cha, L., Xie, C., Feng, Q., et al.: Geometric criteria for the snap-off of a nonwetting droplet in pore-throat channels with rectangular cross-sections. *Water Resour. Res.* **57**, e2020WR029476 (2020)
- Chen, J.D., Wilkinson, D.: Pore-scale viscous fingering in porous media. *Phys. Rev. Lett.* **55**, 1892 (1985)
- Cui, J., Babadagli, T.: Use of new generation chemicals and nano materials in heavy-oil recovery: visual analysis through micro fluidics experiments. *Coll. Surf. A Physicochem. Eng. Asp.* **529**, 346–355 (2017)
- Fisher, M.: Critical probabilities for cluster size and percolation problems. *J. Math. Phys.* **2**, 620–627 (1961)
- Gao, Y., Lin, Q., Bijeljic, B., et al.: Pore-scale dynamics and the multiphase darcy law. *Phys. Rev. Fluids* **5**(013), 801 (2020)
- Gunda, N., Bera, B., Karadimitriou, N., et al.: Reservoir-on-a-chip (roc): a new paradigm in reservoir engineering. *Lab. Chip* **11**, 3785–3792 (2011)
- Gutiérrez, B., Juarez, F., Ornelas, L., et al.: Experimental study of gas-liquid two-phase flow in glass micro-models. *Int. J. Thermophys.* **29**, 2126–2135 (2008)
- Haghighi, M., Xu, B., Yortsos, Y.: Visualization and simulation of immiscible displacement in fractured systems using micromodels: I. drainage. *J. Colloid Interface Sci.* **166**, 168–179 (1994)
- Hashemi, M., Sahimi, M., Dabir, B.: Percolation with two invaders and two defenders: volatile clusters, oscillations, and scaling. *Phys. Rev. Lett.* **80**, 3248 (1998)
- Hashemi, M., Dabir, B., Sahimi, M.: Dynamics of two-phase flow in porous media: simultaneous invasion of two fluids. *AIChE J.* **45**, 1365–1382 (1999)
- Hashemi, M., Sahimi, M., Dabir, B.: Monte carlo simulation of two-phase flow in porous media: invasion with two invaders and two defenders. *Physica A* **267**, 1–33 (1999)
- Heiba, A., Sahimi, M., Scriven, L., et al.: Percolation theory of two-phase relative permeability. *SPE Res. Eng.* **7**, 123–132 (1992)
- Holstvoogd, J.: Analysis of steady multiphase flow in porous media across a hypothetical 2d percolating network. Master's thesis, BSc thesis, Delft U. of Technology, <http://resolver.tudelft.nl/uuid:c94c34c3-e418-4034-831f-df45b32f1d82> (2020)
- Jahanbakhsh, A., Włodarczyk, K., Hand, D., et al.: Review of microfluidic devices and imaging techniques for fluid flow study in porous geomaterials. *Sensors* **20**, 4030 (2020)
- Jeong, S.W., Corapcioglu, M.: A micromodel analysis of factors influencing napl removal by surfactant foam flooding. *J. Contam. Hydrol.* **60**, 77–96 (2003)
- Joekear-Niasar, V., Hassanizadeh, S.M.: Analysis of fundamentals of two-phase flow in porous media using dynamic pore-network models: a review. *Crit. Rev. Environ. Sci. Tech.* **42**, 1895–1976 (2012)
- Karadimitriou, N., Hassanizadeh, S.M.: A review of micromodels and their use in two-phase flow studies. *Vadose Zone J.* **11**(vzj2011), 0072 (2012)
- Karadimitriou, N., Musterd, M., Kleingeld, P., et al.: On the fabrication of pdms micromodels by rapid prototyping, and their use in two-phase flow studies. *Water Resour. Res.* **49**, 2056–2067 (2013)

- Kazemifar, F., Blois, G., Kyritsis, D., et al.: Quantifying the flow dynamics of supercritical co₂-water displacement in a 2d porous micromodel using fluorescent microscopy and microscopic piv. *Adv. Water Resour.* **95**, 352–368 (2016)
- Kennedy, C., Lennox, W.C.: A pore-scale investigation of mass transport from dissolving dnapi droplets. *J. Contam. Hydrol.* **24**, 221–246 (1997)
- King, P., Masihi, M.: *Percolation Theory in Reservoir Engineering*. World Scientific Publishing Europe Ltd (2019)
- Kovscek, A., Tang, G.Q., Radke, C.: Verification of roof snap off as a foam-generation mechanism in porous media at steady state. *Colloid Surf. A Physicochem. Eng. Asp.* **302**, 251–260 (2007)
- Lago, M., Araujo, M.: Threshold pressure in capillaries with polygonal cross section. *J. Colloid Interface Sci.* **243**, 219–226 (2001)
- Lake, L., Johns, R., Rossen, W., et al.: *Fundam. Enhanc. Oil Recov.* Society of Petroleum Engineers, Richardson, TX (2014)
- Lenormand, R., Zarcone, C., Sarr, A.: Mechanisms of the displacement of one fluid by another in a network of capillary ducts. *J. Fluid Mech.* **135**, 337–353 (1983)
- Ma, S., Mason, G., Morrow, N.: Effect of contact angle on drainage and imbibition in regular polygonal tubes. *Colloid Surface A Physicochem. Eng. Asp.* **117**, 273–291 (1996)
- Marafini, E., La Rocca, M., Fiori, A., et al.: Suitability of 2d modelling to evaluate flow properties in 3d porous media. *Transp. Porous Media* **134**, 315–329 (2020)
- Marchand, S., Bondino, I., Ktari, A., et al.: Consideration on data dispersion for two-phase flow micromodel experiments. *Transp. Porous Med.* **117**, 169–187 (2017)
- Mohanty, K., Davis, H., Scriven, L.: Physics of oil entrapment in water-wet rock. *SPE Res. Eng.* **2**, 113–128 (1987)
- Morais, S., Cario, A., Liu, N., et al.: Studying key processes related to co₂ underground storage at the pore scale using high pressure micromodels. *React. Chem. Eng.* **5**, 1156–1185 (2020)
- Øren, P.E., Bakke, S., Arntzen, O.: Extending predictive capabilities to network models. *SPE J.* **3**, 324–336 (1998)
- Paterson, L.: Diffusion-limited aggregation and two-fluid displacements in porous media. *Phys. Rev. Lett.* **52**, 1621 (1984)
- Perez, L., Parashar, R., Plymale, A., et al.: Contributions of biofilm-induced flow heterogeneities to solute retention and anomalous transport features in porous media. *Water Res.* **209**(117), 896 (2022)
- Peters, E.: *Advanced Petrophysics*, vol. 2. Live Oak Book Co., Austin, TX (2012)
- Ransohoff, T., Radke, C.: Laminar flow of a wetting liquid along the corners of a predominantly gas-occupied noncircular pore. *J. Colloid Interface Sci.* **121**, 392–401 (1989)
- Ransohoff, T., Radke, C.: Mechanisms of foam generation in glass-bead packs. *SPE Res. Eng.* **3**, 573–585 (1989)
- Ransohoff, T., Gauglitz, P., Radke, C.: Snap-off of gas bubbles in smoothly constricted noncircular capillaries. *AIChE* **33**, 753–765 (1987)
- Roman, S., Soulaïne, C., AlSaud, M.A., et al.: Particle velocimetry analysis of immiscible two-phase flow in micromodels. *Adv. Water Resour.* **95**, 199–211 (2016)
- Roman, S., Abu-Al-Saud, M., Tokunaga, T., et al.: Measurements and simulation of liquid films during drainage displacements and snap-off in constricted capillary tubes. *J. Colloid Interface Sci.* **507**, 279–289 (2017)
- Roof, J.: Snap-off of oil droplets in water-wet pores. *SPE J.* **10**, 85–90 (1970)
- Rossen, W.: A critical review of Roof snap-off as a mechanism of steady-state foam generation in homogeneous porous media. *Colloid Surf. A Physicochem. Eng. Asp.* **225**, 1–24 (2003)
- Rossen, W.: Comment on verification of roof snap-off at a foam-generation mechanism in porous media at steady state. *Colloid Surf. A Physicochem. Eng. Asp.* **322**, 261–269 (2008)
- Sahimi, M.: *Applications of Percolation Theory*. CRC Press (1994)
- Selyakov, V., Kadet, V.: *Percolation Models for Transport in Porous Media: With Applications to Reservoir Engineering*. Kluwer Academic Publishers (1996)
- Shikhov, I., Arns, C.: Evaluation of capillary pressure methods via digital rock simulations. *Transp. Porous Med.* **107**, 623–640 (2015)
- Tang, J., Smit, M., Vincent-Bonnieu, S., et al.: New capillary number definition for micromodels: the impact of pore microstructure. *Water Resour. Res.* **55**, 1167–1178 (2019)
- Valvatne, P., Blunt, M.: Predictive pore-scale modeling of two-phase flow in mixed wet media. *Water Resour. Res.* **40**(W07), 406 (2004)
- Wu, Y., Fang, S., Dai, C., et al.: Investigation on bubble snap-off in 3-D pore-throat micro-structures. *J. Ind. Eng. Chem.* **54**, 69–74 (2017)

- Zhang, Y., Bijeljic, B., Gao, Y., et al.: Quantification of nonlinear multiphase flow in porous media. *Geophys. Res. Lett.* **48**, e2020GL090477 (2021)
- Zhao, B., MacMinn, C., Juanes, R.: Wettability control on multiphase flow in patterned microfluidics. *Proc. Natl. Acad. Sci.* **113**, 10251–10256 (2016)

Publisher's Note Springer Nature remains neutral with regard to jurisdictional claims in published maps and institutional affiliations.